International Journal of Minerals, Metallurgy and Materials
Volume 23, Number 12, December 2016, Page 1416
DOI: 10.1007/s12613-016-1365-2

Influence of shielding gas on the mechanical and metallurgical properties of DP-GMA-welded 5083-H321 aluminum alloy

Amin Reza Koushki[1)], *Massoud Goodarzi*[1)], *and Moslem Paidar*[2)]

1) Department of Metallurgy and Materials Engineering, Iran University of Science and technology, Tehran, Iran
2) Department of Materials Engineering, South Tehran Branch, Islamic Azad University, Tehran, Iran
(Received: 27 May 2016; revised: 5 October 2016; accepted: 11 October 2016)

Abstract: In the present research, 6-mm-thick 5083-H321 aluminum alloy was joined by the double-pulsed gas metal arc welding (DP-GMAW) process. The objective was to investigate the influence of the shielding gas composition on the microstructure and properties of GMA welds. A macrostructural study indicated that the addition of nitrogen and oxygen to the argon shielding gas resulted in better weld penetration. Furthermore, the tensile strength and bending strength of the welds were improved when oxygen and nitrogen (at concentrations as high as approximately 0.1vol%) were added to the shielding gas; however, these properties were adversely affected when the oxygen and nitrogen contents were increased further. This behavior was attributed to the formation of excessive brown and black oxide films on the bead surface, the formation of intermetallic compounds in the weld metal, and the formation of thicker oxide layers on the bead surface with increasing nitrogen and oxygen contents in the argon-based shielding gas. Analysis by energy-dispersive X-ray spectroscopy revealed that most of these compounds are nitrides or oxides.

Keywords: aluminum alloys; gas metal arc welding; shielding gas; mechanical properties; metallurgical properties

1. Introduction

Welding is a joining method selected mainly for assembling large metal structures such as ships, bridges, construction machinery, and aircraft. Among various fusion welding processes, the gas metal arc welding (GMAW) process is one of the most widely used methods because it suits a wide range of applications [1]. The GMAW process is very widely used in industry and involves heating, melting, and solidification of base metals and a filler (wire electrode) material in a restricted fusion zone by a transient heat source to form a weld between the base metals [2].

Recently, a new welding technique has been developed as a derivative of the pulsed GMAW (P-GMAW), which is GMAW with a low-frequency current pulsation. This new technique is named double-pulsed GMAW (DP-GMAW). In the DP-GMAW method, the pulsing current used to control metal transfer is overlapped by a thermal pulsation, which is used for pool control [3]. The most commonly used shielding gas in this process for welding Al alloys is Ar, which is inert and relatively inexpensive; as a shielding gas, the Ar prevents oxidation of the molten metal. The GMAW welding parameters influence the quality, productivity, and cost of welding joints. These parameters comprise the welding current, arc voltage, welding speed, torch angle, nozzle-to-plate distance, welding position and direction, flow rate, and the shielding gas composition [2].

A few studies dealing with DP-GMAW of Al alloys have been reported. For instance, Mendes Da Silva and Scotti [3] reported a comparative study between the P-GMAW and DP-GMAW techniques in relation to formation of pores in welded 5052 Al alloy. They found that, compared to the pulsed GMAW technique, the DP-GMAW technique, despite having a theoretically greater potential for pore generation, did not increase the susceptibility of the Al to pore formation during welding. Anttila and Porter [4] investigated the effect of shielding gas mixtures of Ar, N_2, and O_2 in welds of stabilized 21wt% Cr ferritic stainless steel in autogenous gas tungsten arc welding (GTAW) and laser welding to explore the possibility of inducing grain refine-

Corresponding author: Moslem Paidar E-mail: M.paidar@srbiau.ac.ir

ment. They found that N_2 addition alone was inadequate because O_2 was needed to produce oxide inoculants for nitrides and to produce a uniform slag to protect the solidifying weld pool surface from N_2 outgassing. Notably, laser welding did not produce similar features in the weld metals.

Some researchers have also investigated the effect of the shielding gas composition on the microstructure and mechanical properties of samples welded using the GMAW, GTAW, and flux cored arc welding (FCAW) processes. For example, Mvola and Kah [5] investigated the effect of shielding gas control on the metallurgical and mechanical properties in GMA welding. They found that the shielding gas was a major factor in determining weld joint properties. They also reported that the addition of NO, CO_2, or He to Ar at concentrations less than 0.03vol% improved the stability of the arc welding process and improved the quality of the resulting welded joints.

Liskevych and Scotti [6] investigated the effect of the CO_2 content in Ar-based shielding gas on the operational performance of short-circuit GMAW. Their results showed that increasing CO_2 content in the shielding gas adversely affected the metal transfer regularity and led to excessive spatter generation and uneven bead appearance. Huang [7] investigated the effects of shielding-gas composition on weld morphology and mechanical properties in the GTAW process. They reported that increasing the N_2 content in the shielding gas increased the tensile strength, hardness, and the weld penetration depth. Moreover, Prokić-Cvetković *et al.* [8] explored the effect of shielding-gas composition on the toughness and crack growth parameters of AlMg4.5Mn weld metals and reported that increasing the amount of He in the shielding gas resulted in increases in the impact energy and the crack growth energy and a decrease in the crack growth rate.

Boukha *et al.* [9] studied the influence of CO_2–Ar mixtures as the shielding gas on laser welding of AA5083 aluminum alloy. Their results showed that the addition of CO_2 to the shielding gas mixture in the laser welding process did not modify the microstructure of the 5083 aluminum alloy, whereas the addition of small percentage of CO_2 to Ar led to improvements in the mechanical and corrosion properties of the Al welds.

Arivazhagan *et al.* [10] investigated the effect of shielding gas composition on the toughness of flux-cored arc welding of modified 9Cr–1Mo (P91) steel and found that, among the four different shielding gases studied, 95vol% Ar + 5vol% CO_2 was the best shielding gas mixture for producing sound welds with high toughness and better operating characteristics. Murphy *et al.* [11] studied the effect of adding He, H_2, and N_2 to Ar shielding gas. They discovered that the shear stress and the arc pressure at the anode surface increased with the addition of H_2 or N_2 but decreased when more He was added. De Salazar *et al.* [12] investigated the effect of N_2 addition in the MIG welding process of duplex steels. They concluded that the optimal content of N_2 in the shielding gas was between 3vol% and 5vol%.

Given these results and the differences in the findings reported by various researchers, the effect of shielding gas composition on the metallurgical and mechanical properties of welds made by DP-GMAW should be intensively investigated. The objective of this study was to determine the influence of shielding gas composition on the mechanical properties (tensile and bending strength) of the welded joint on 5083-H321 and to compare the influence of the shielding gas composition on the microstructure and macrostructure of welded joints.

2. Experimental

The material to be welded was 5083-H321 Al alloy. The dimensions of the Al alloy plates were 200 mm × 70 mm × 10 mm for the bead-on-plate welding experiments, whereas the dimensions of the Al alloy plates for the single V-groove welding experiments were 320 mm × 150 mm × 6 mm. Fig. 1 shows a schematic of the experimental setup used in this study (butt-joint V-groove). Tables 1 and 2 show the chemical analysis and mechanical properties of the alloy, respectively. Al based filler metal 5183 with a diameter of 1.2 mm was used. Notably, the process was conducted at a constant flow rate of 21 L/min and a welding speed of

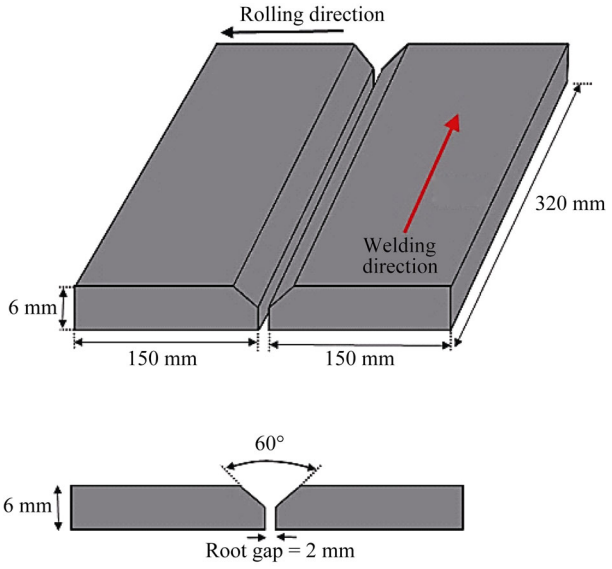

Fig. 1. Schematic illustration of the experimental set up used for this study.

Table 1. Chemical composition of 5083-H321 aluminum alloy

wt%

Al	Mg	Mn	Fe	Cr	Si
Base	4.31	0.63	0.23	0.12	0.11

Table 2. Mechanical properties of 5083-H321 aluminum alloy

Ultimate tensile / MPa	Yield strength / MPa	Elongation / %
320	153	18.1

40 cm/min for all samples. In addition, the angle between the nozzle and the vertical line was maintained at 20°.

The welds were made using a ProMIG 511 welder, which is shown in Fig. 2. Notably, the weld line was perpendicular to the rolling direction of the as-received materials. The sample welds were made in the flat position. Four types of shielding gases were used in this study, and the experimental results were compared. The type of shielding gases used in the trials is summarized in Table 3. The geometries of the tensile and bending test specimens were selected according to standard ASTM D 1.2 to investigate the GMA welds. For each weld joint, three tensile specimens were collected. The geometry of the tensile test specimens is illustrated in Fig. 3.

The tensile tests were conducted at room temperature on an INSTRON 5500R materials testing system using a cross-head speed of 5 mm/min. In preparation for metallography, the specimens were polished to a mirror-like finish and then etched using Keller's reagent (1.0 mL HF, 1.5 mL HCl, 2.5 mL HNO_3, and 95.0 mL H_2O) for 12 s to reveal the microstructure of the joints. In addition, a scanning electron microscope equipped with an energy-dispersive X-ray spectrometer (VEGA TESCAN) and an optical microscope (Olympus CK40) were used to detect and measure the penetration and width of the welds and to characterize their microstructure, respectively. The thicknesses of the oxide layers were measured using the XPS MultiQuant 7.0 program utilizing the oxide-layer model. An image analyzer program was used to evaluate the size of the grains.

3. Results and discussion

3.1. Macrostructure and appearance of joints

The images of weld surfaces generated by DP-GMAW of 5083-H321 aluminum alloy using Ar shielding gas with

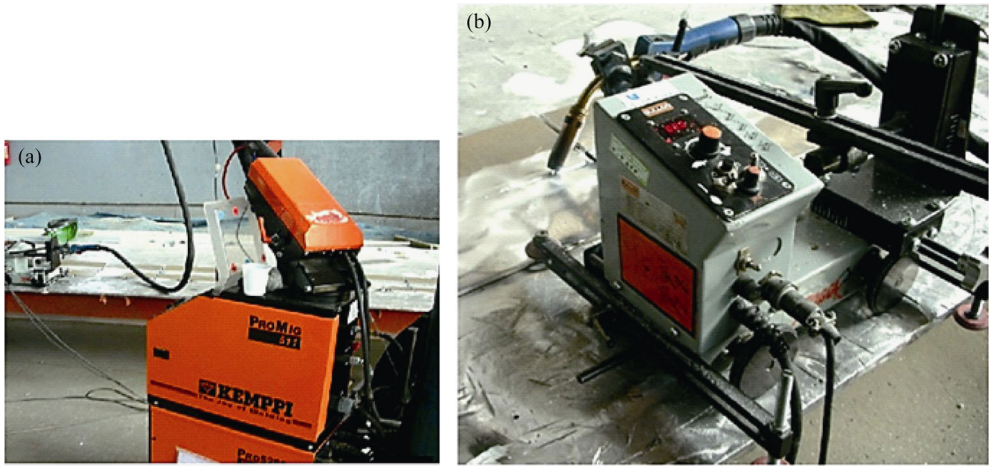

Fig. 2. (a) Automatic DP-GMAW machine for welding; (b) close-up view of the specimens.

Table 3. Shielding gases used in this study

No	Shielding gas
1	100% Ar
2	Ar–0.03vol%NO
3	Ar–0.1vol%N_2–0.1vol%O_2
4	Ar–0.5vol%N_2–0.5vol%O_2
5	Ar–0.5vol%N_2–1vol%O_2
6	Ar–1vol%N_2–1vol%O_2
7	Ar–1vol%N_2–2vol%O_2
8	Ar–2vol%N_2–2vol%O_2

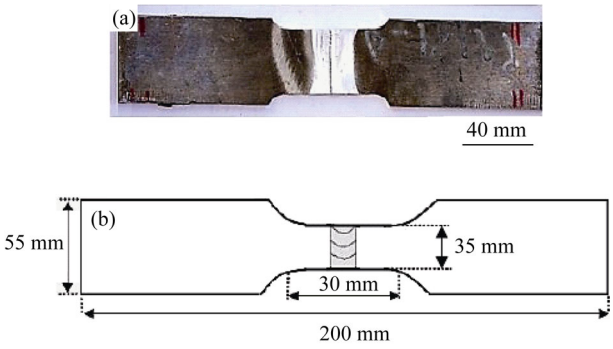

Fig. 3. (a) Shape and (b) size of the tensile test samples prepared from welds in this study.

different N_2 and O_2 contents are shown in Fig. 4. A comparison of Figs. 4(a) to 4(c) indicates that the use of the different shielding gases tended to create excessive spatters and oxides on the surface of the welds in comparison to the welds formed using pure Ar. These oxides act as a barrier for the shielding gas conveyance to the weld metal [9]. As evident from the results in Fig. 4, the use of Ar–0.03vol%NO as shielding gas resulted in a clean weld bead surface. Because NO gas has an ionization potential (9.70 eV) lower than that of Ar gas (15.8 eV), the addition of NO to the Ar beneficially affected the weld surface, which was relatively clean (see Fig. 4(b)). Moreover, the observed increase in the concentrations of oxides on the weld surface is related to changes in the heat flow as a function of the shielding gas composition. This higher heat flow can relatively increase the heat input of the welds.

The obtained results also clearly show that the addition of N_2 and O_2 to the Ar-based shielding gas resulted in an oxide layer on the weld surface. A continuous oxide layer covered the bead surface, and a heavy oxide layer formed in the periphery area of the weld surface when the N_2 and O_2 were added to the Ar shielding gas. Notably, the thickness of the oxide layers changed as a function of the shielding gas composition. Accordingly, when the Ar–2vol%O_2– 2vol%N_2 gas was used, a thicker oxide layer formed on the weld surface; by contrast, when the Ar–0.1vol%O_2– 0.1vol%N_2 gas was used, a thinner oxide layer formed on the weld surface. On the basis of the aforementioned results, we concluded that increasing the content of N_2 and O_2 gases in the -based shielding gas leads to variation in the thickness of oxide layers on the weld surface, which suggests that the shielding gas strongly affects both the weld surface and the thickness of oxide layers on the weld surface.

The oxide layer on the weld surface was analyzed by scanning electron microscopy (SEM) and energy-dispersive X-ray spectroscopy (EDS) (Fig. 5). The results indicate that the oxide layer was composed predominantly of nitrogen and oxygen. The O_2 and N_2 in the shielding gas reacted with the Al.

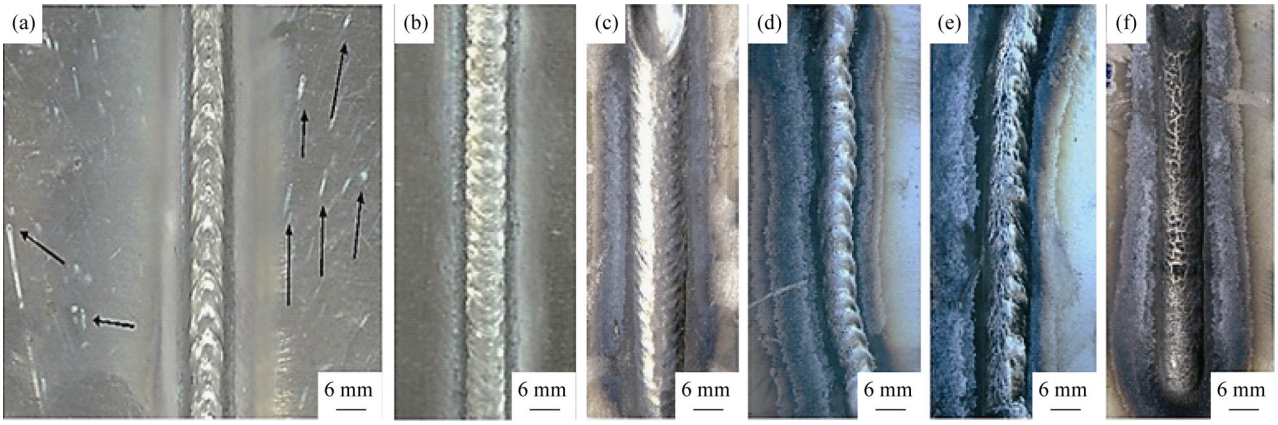

Fig. 4. Relationship between shielding gas composition and bead surface: (a) pure Ar; (b) Ar–0.03vol%NO; (c) Ar–0.1vol%N_2–0.1vol%O_2; (d) Ar–0.5vol%N_2–1vol%O_2; (e) Ar–1vol%N_2–2vol%O_2; (f) Ar–2vol%N_2–2vol%O_2.

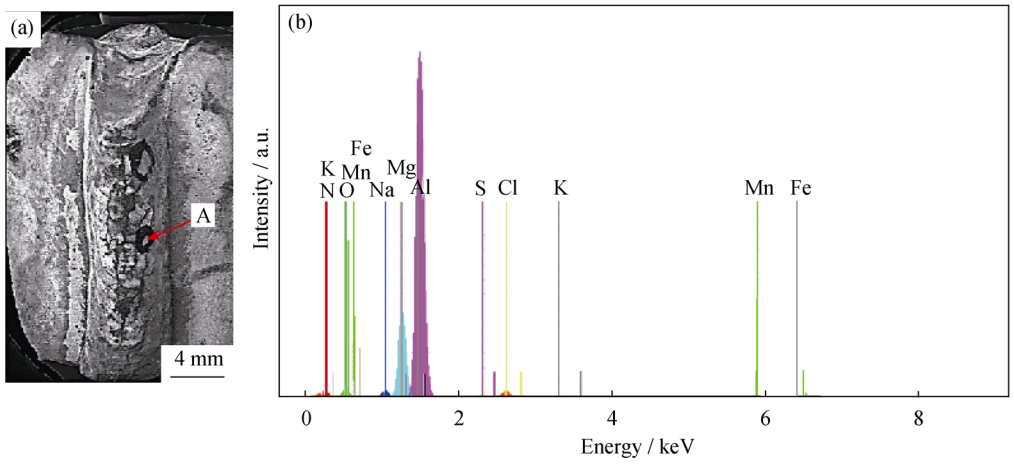

(c)

Element	Concent / wt%
Nitrogen	8.78
Oxygen	11.31
Sodium	1.85
Magnesium	16.72
Aluminum	59.26
Sulfur	0.28
Chlorine	0.96
Potasium	0.30
Manganese	0.42
Iron	0.11

Fig. 5. (a) SEM micrograph of a weld made with Ar–2vol%N_2–2vol%O_2 shielding gas, (b) EDS spectrum of region A, and (c) EDS results of region A.

Macroscopic images of the cross-sections of weld beads formed under different N_2 and O_2 concentrations in the shielding gas are included in Figs. 6 and 7. The results in these figures show that increasing N_2 and O_2 concentrations in the shielding gas resulted in increased weld penetration. Indeed, welds formed under shielding gas with low N_2 and O_2 contents exhibited a wide and shallow morphology. For instance, the penetration of the weld joint formed with 0.03vol% NO in the Ar-based shielding gas was approximately 21% deeper compared to that formed under pure Ar shielding gas; this greater penetration is attributable to the higher arc voltage obtained with Ar–0.03vol%NO shielding gas, although this behavior might also originate from the Marangoni convection effect. In fact, the addition of NO, N_2, and O_2 to the Ar-based shielding gas caused the temperature coefficient of the surface tension to change from a negative to a positive value, thereby reversing the Marangoni convection direction in the weld pool and resulting in a deep weld shape. Furthermore, the greater penetration could be associated with the reaction that occurs between Al and the N_2 and O_2 gases:

$2Al + N_2 = 2AlN$, $\Delta G = -424$ kJ at 1000°C,

$\Delta G = -200$ kJ at 2000°C.

$2Al + \frac{3}{2}O_2 = Al_2O_3$, $\Delta G = -1361$ kJ at 1000°C,

$\Delta G = -1034$ kJ at 2000°C.

These reactions are highly exothermic, and the heat released in the fusion zone would lead to enhanced weld penetration depth.

On the basis of the aforementioned results, the composition of the shielding gas strongly affected both the penetration depth and the surface appearance of the welds. In fact, the addition of N_2 and O_2 to the shielding gas increased the heat input, resulting in increased weld penetration. These results indicate that increasing the N_2, O_2, and NO contents in the Ar-based shielding gas not only affected the macrostructure of the welds but also affected the angular distortion and, consequently, the mechanical properties of the welded joints. Anttila and Porter [4] investigated the effect of shielding gases on grain refinement in welds formed by GTAW of stabilized 21wt% Cr ferritic stainless steel. They found that the use of N_2 as a shielding gas component led to extensive nitride precipitation in GTA welds and, subsequently, to a reduction in impact energy.

3.2. Microstructure studies

Fig. 8 reveals the microstructures of different regions in the DP-GMA welds. The cross-sections of the DP-GMA welds were divided into three regions: the heat-affected zone (HAZ), the weld metal (WM), and the parent metal (PM). As evident in Fig. 8, grains in the weld metal were oriented parallel to the heat flow [13].

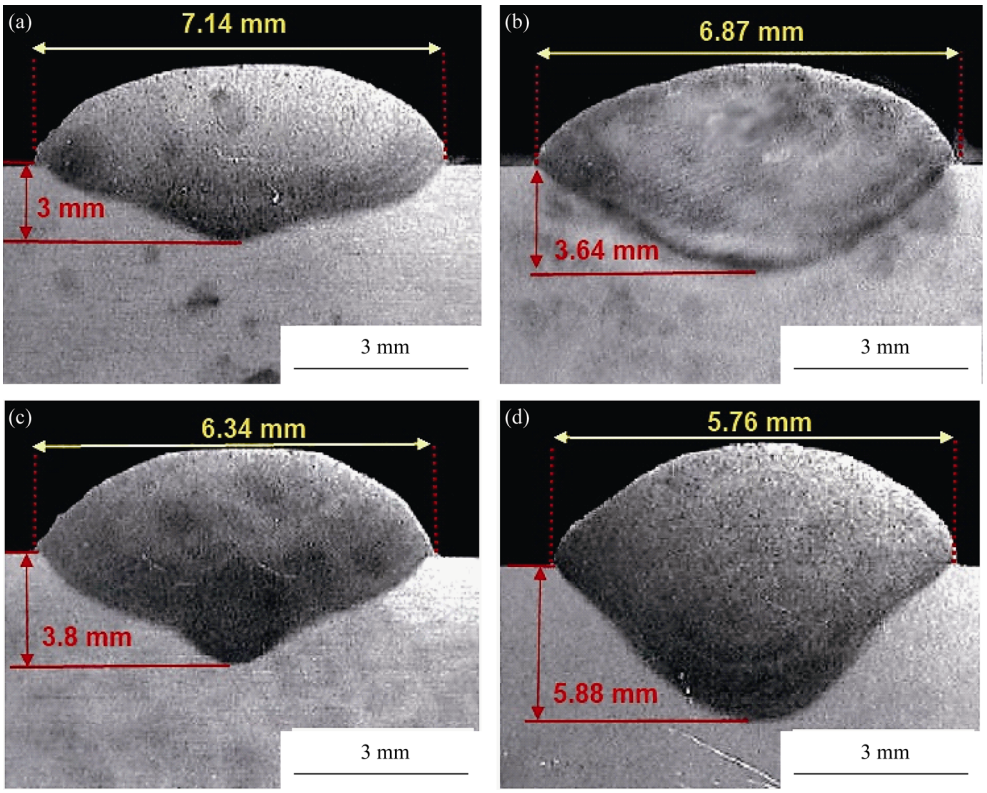

Fig. 6. Effect of nitrogen and oxygen addition on the morphology of DP-GMAW of AA5083-H321: (a) pure Ar; (b) Ar–0.03vol%NO; (c) Ar–0.1vol%N_2–0.1vol%O_2; (d) Ar–1vol%N_2–2vol%O_2.

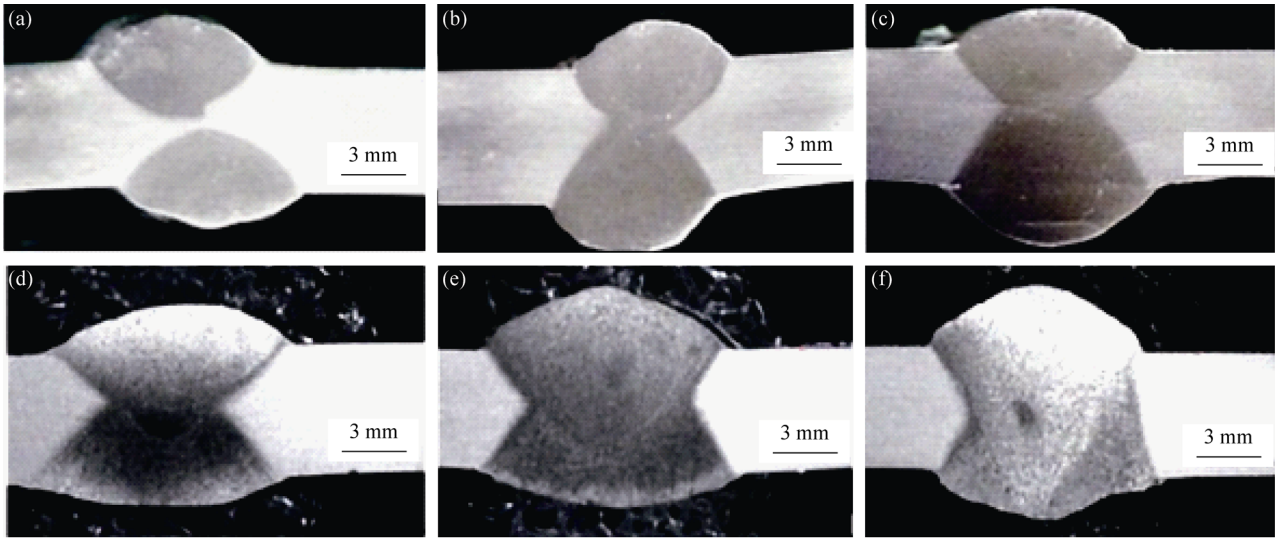

Fig. 7. Effect of nitrogen and oxygen addition on the morphology of DP-GMAW of AA5083-H321 aluminum alloy: (a) pure Ar; (b) Ar–0.03vol%NO; (c) Ar–0.1vol%N_2–0.1vol%O_2; (d) Ar–0.5vol%N_2–1vol%O_2; (e) Ar–1vol%N_2–1vol%O_2; (f) Ar–1vol%N_2–2vol%O_2.

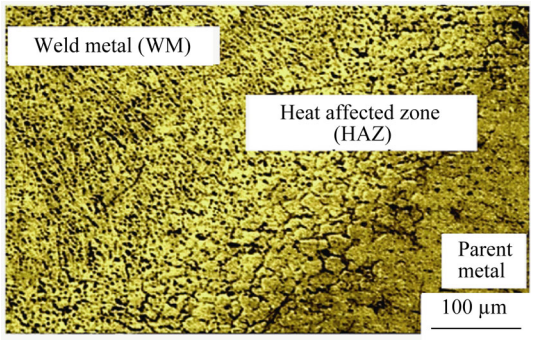

Fig. 8. Microstructure of different regions in DP-GMAW under pure Ar shielding gas.

Fig. 9 compares the influence of the shielding gas composition (pure Ar compared to Ar–0.03vol%NO) on the microstructure of the WM and the HAZ. As evident in Figs. 9(a) and 9(d), an equiaxed dendritic structure formed in the WM regardless of the type of shielding gas; this structure corresponds to the zones with higher resolidification rates [9]. Additionally, a finer grain size was obtained in the HAZ for welds formed under pure Ar (approximately 63 μm), whereas the average grain size in the HAZ of welds made with Ar–0.03vol%NO was approximately 70 μm. This difference in grain size is explained by differences in the arc voltage. As previously discussed, the arc voltage increased when 0.03vol% NO was added to the Ar shielding gas, which led to an enhancement of the weld penetration. In fact, when the arc voltage increased, the generated heat input increased, which caused grain growth. Fig. 9 also shows that the size of precipitates decreased considerably as NO was added to the Ar-based shielding gas (precipitates might have dissolved after welding), resulting in a better dispersion of precipitates in the WM.

The relationship between shielding gas composition and the microstructure of the WM and the HAZ is represented in Fig. 10. This figure clearly shows that the microstructure of the weld changed as the type of shielding gas was varied. Fig. 10 also shows that both the grain sizes and the amount of intermetallic compounds (IMCs) in Ar–N_2–O_2-GMA welded joints compared to those in the pure Ar GMA welded joints increased with increasing N_2 and O_2 contents in the shielding gas. Importantly, as the N_2 and O_2 contents were increased from 0.1vol% to 2vol%, precipitates accumulated, indicating that the number of detected defects increased with increasing proportions of N_2 and O_2 gases. As shown in Table 4, the HAZ of welds formed using shielding gas with low N_2 and O_2 contents have finer grain sizes than welds formed using shielding gas with high N_2 and O_2 contents. We thus conclude that the presence of O_2, N_2, and NO in the Ar shielding gas substantially affects the microstructure of the WM and the HAZ. Furthermore, our results indicate that an optimal set of conditions exist for obtaining the best microstructure and that excess N_2 and O_2 led to growth of IMCs in the HAZ and the WM, whereas the addition of 0.03vol% NO to the Ar shielding gas improved the microstructure of the resulting welded joints.

Fig. 11 shows the SEM backscattered electron (BSE) images of welds obtained using different shielding gases and compares the influence of the shielding gas composition on the chemical composition of the phases obtained during DP-GMAW. EDS was used to compare the different IMC phases formed in these joints. The region A layer was found to have a composition of approximately 10.57wt% Al, 57.31wt% Mg, 29.49wt% Si, and 2.52wt% O and likely formed an $Mg_2Al_3 + Mg_2Si$ phase. Region B exhibited a com-

position of approximately 75.07wt% Al, 8.61wt% Mn, and 12.32wt% Fe and likely formed $Al_6(Fe,Mn)$. Region D exhibited a composition of approximately 47.26wt% Al, 0.13wt% Fe, 14.06wt% O, and 9.56wt% N and likely formed an $AlMg_xO_xN_x$ phase; thus, the results also indicate that this region is rich in nitrogen. Region E exhibited a composition of approximately 50.79wt% Al, 4.77wt% Mg, 0.40wt% Fe, 6.28wt% O, and 29.68wt% N and likely formed an AlN phase.

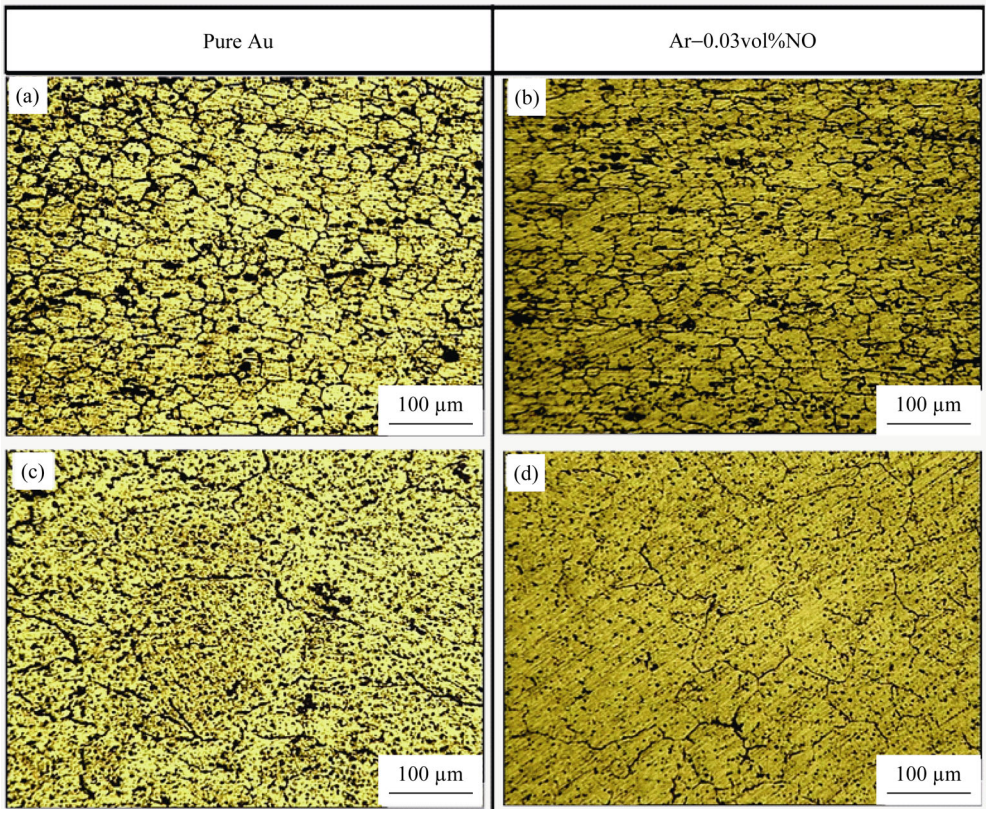

Fig. 9. Microstructures of (a) HAZ under 100% Ar shielding gas, (b) HAZ under Ar–0.03vol%NO shielding gas, (c) WM under 100% Ar shielding gas, and (d) WM under Ar–0.03vol%NO shielding gas.

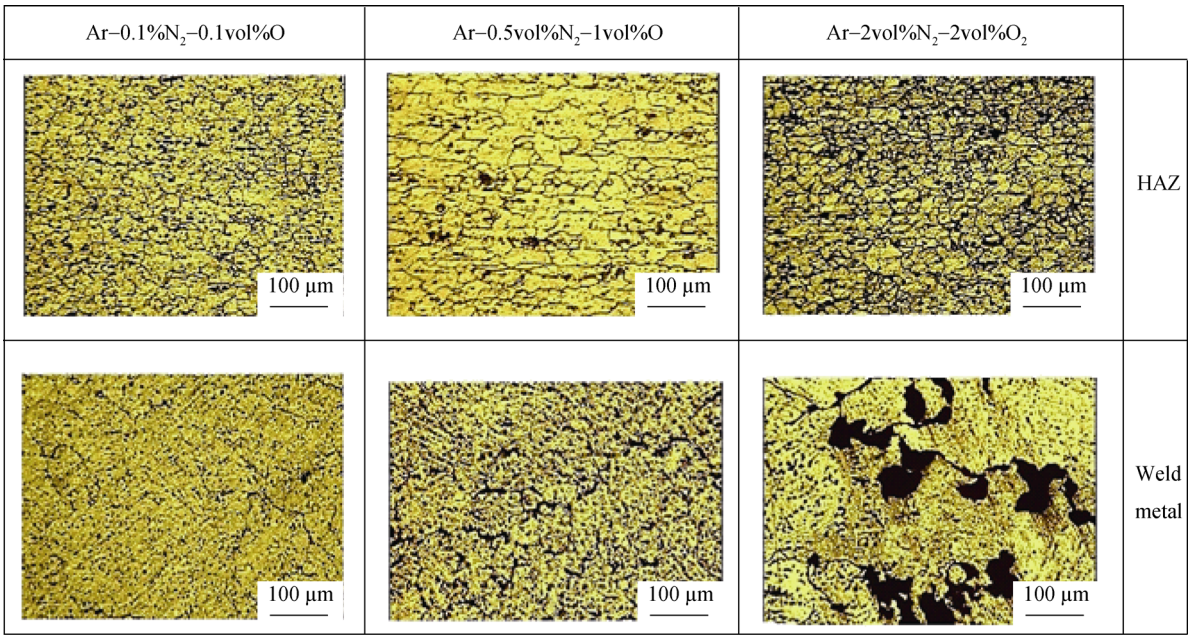

Fig. 10. Optical images of the microstructures of the WM and HAZ in welding joints of GMA welded 5083 aluminum alloy joints with different shielding gases.

Table 4. Average grain sizes in the heat-affected zone (HAZ)

Shielding gas	Average grain size / μm
100% Ar	63.5
Ar–0.03vol%NO	69.0
Ar–0.1vol%N–0.1vol%O	71.0
Ar–0.5vol%N–1vol%O	89.8
Ar–2vol%N–2vol%O	95.0

IMCs are well known to be very brittle and to subsequently affect the tensile strength of joints. The EDS analysis results indicate that the shielding gas strongly affected the formation of IMCs in welded joints during DP-GMAW of AA5083-H321.

3.3. Mechanical properties

The mechanical properties of the joints were characterized by bending tests and tensile tests. Tensile and bending tests were performed to evaluate the effect of the shielding gas composition on the tensile and bending strengths. Fig. 12 depicts the effect of shielding gas composition on the ultimate tensile strength (UTS) of welded specimens. The addition of N_2 and O_2 to Ar-based shielding gases is well known to change the UTS of the resulting weld. Fig. 12 clearly shows that N_2 and O_2 added to the Ar-based shielding gas bilaterally affected the UTS. That is, increasing of the N_2 and O_2 content in the shielding gas initially resulted in welds with a greater UTS, but the UTS rapidly decreased as the N_2 and O_2 content was increased further. This sudden decrease in the UTS and yield strength (YS) is explained by the absorption of N_2 during welding and by grain coarsening in the weld metal. N_2 absorbed during welding is known to result in interstitial solid-solution strengthening, thereby simultaneously improving the tensile strength [7,14]. Kuk *et al.* [1] reported that varying the shielding gas composition did not substantially affect the mechanical properties of Al5083 GMA welds. Our results show that the best results were obtained with the Ar–0.1vol%N_2–0.1vol%O_2 shielding gas, which resulted in welds with an average tensile strength of approximately 308 MPa, whereas the worst results were obtained with the Ar–2vol%N_2–2vol%O_2 shielding gas, which resulted in welds with an average tensile strength of approximately 220 MPa. Huang [7] reported that N_2 is one of the most effective elements for increasing the strength of joints.

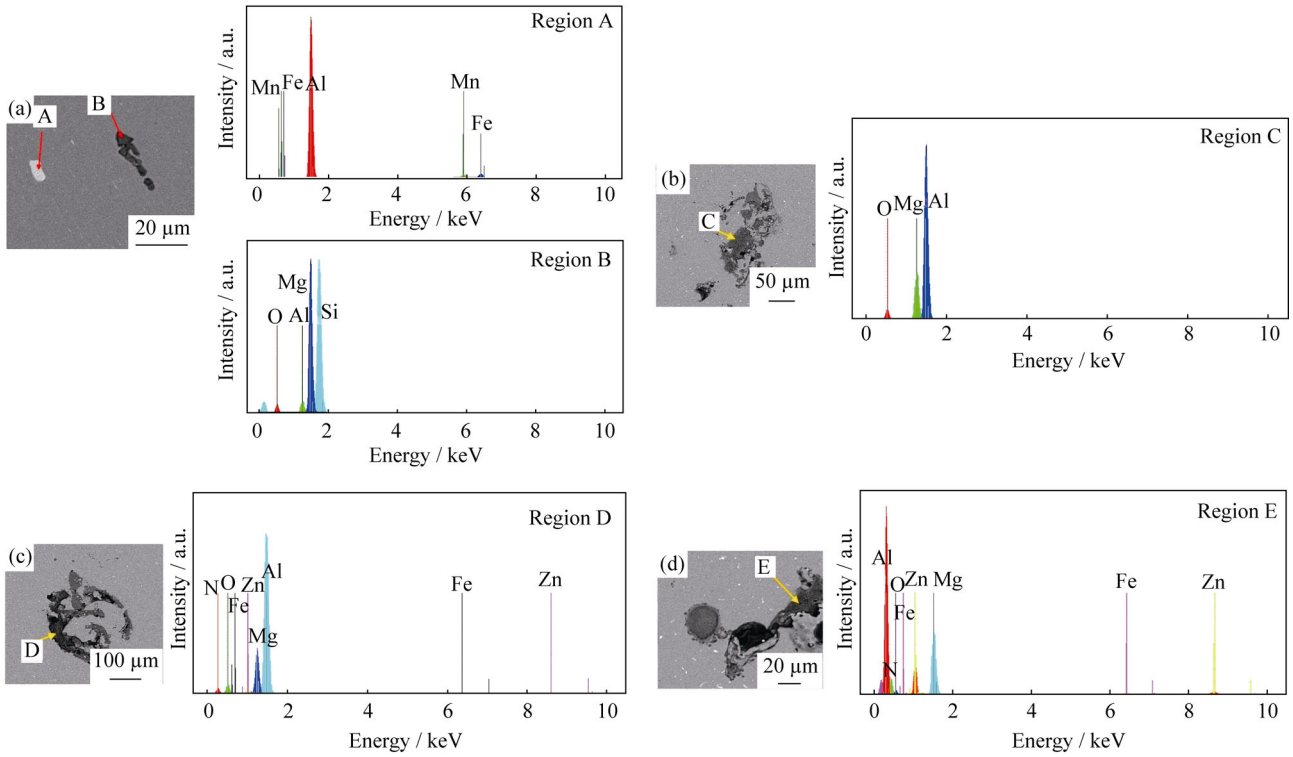

Fig. 11. SEM micrographs of the fusion zone and EDS spectra of regions A, B, C, D and E as a function of shielding gas: (a) pure Ar; (b) Ar–0.03vol%NO; (c) Ar–0.1vol%N_2–0.1vol%O_2; (d) Ar–1vol%N_2–2vol%O_2.

In summary, the additions of N_2, O_2, and NO to the shielding gas effectively increased the UTS and the YS of welded specimens; these improvements are attributed to the finer size of precipitates and to a better dispersion of precipitates in the WM when NO, N_2, and O_2 were added to the Ar-based shielding gas. However, further increases in the N_2

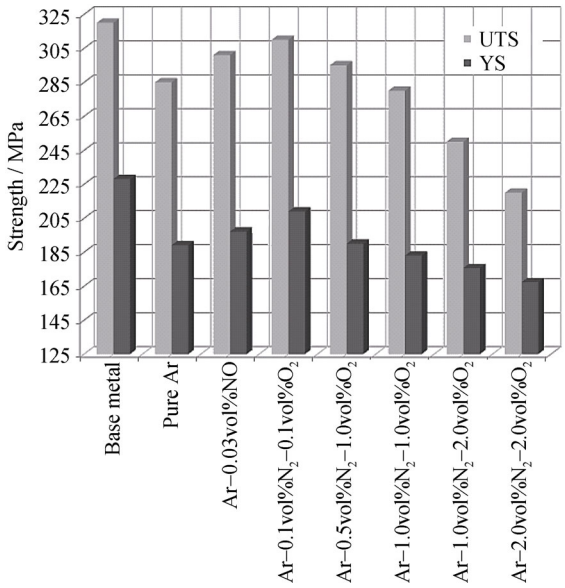

Fig. 12. Effect of shielding gas composition on UTS and YS.

and O_2 content in the shielding gas resulted in a decrease in the UTS. In fact, the addition of N_2 and O_2 led to an increase in the weld penetration depth; however, as previously mentioned, the thickness of oxide layers on the weld surface increased, which adversely affected the mechanical properties of the resulting welded joints. According to the aforementioned results, we concluded that the oxide layers affected the mechanical properties of welded joints more strongly than the weld morphology. Notably, the welding parameters in the present work did not influence fracture location. That is, in all specimens, tensile failure occurred in the WM.

We observed the fractured surfaces of the welds obtained using Ar–0.03vol%NO, Ar–0.1vol%N_2–0.1vol%O_2, Ar–1vol%N_2–2vol%O_2 and Ar–2vol%N_2–2vol%O_2 shielding gas by SEM (Fig. 13) to elucidate the failure patterns. We clearly observed that the fracture surface obtained using Ar–0.03vol%NO includes voids and fine dimples; these fine dimples demonstrate that the fracture mode was ductile. These fine dimples may have originated from the presence of numerous fine precipitates and may also be related to the better dispersion of precipitates. Notably, all of the dimples exhibit an approximately equiaxed pattern. Moreover, the dimple content clearly decreased as the N_2 and O_2 content in the shielding gas was increased. By contrast, a cleavage-type fracture mode was observed in the specimen welded using Ar–2vol%N_2–2vol%O_2 (Fig 13(d)). Fig. 13(d)

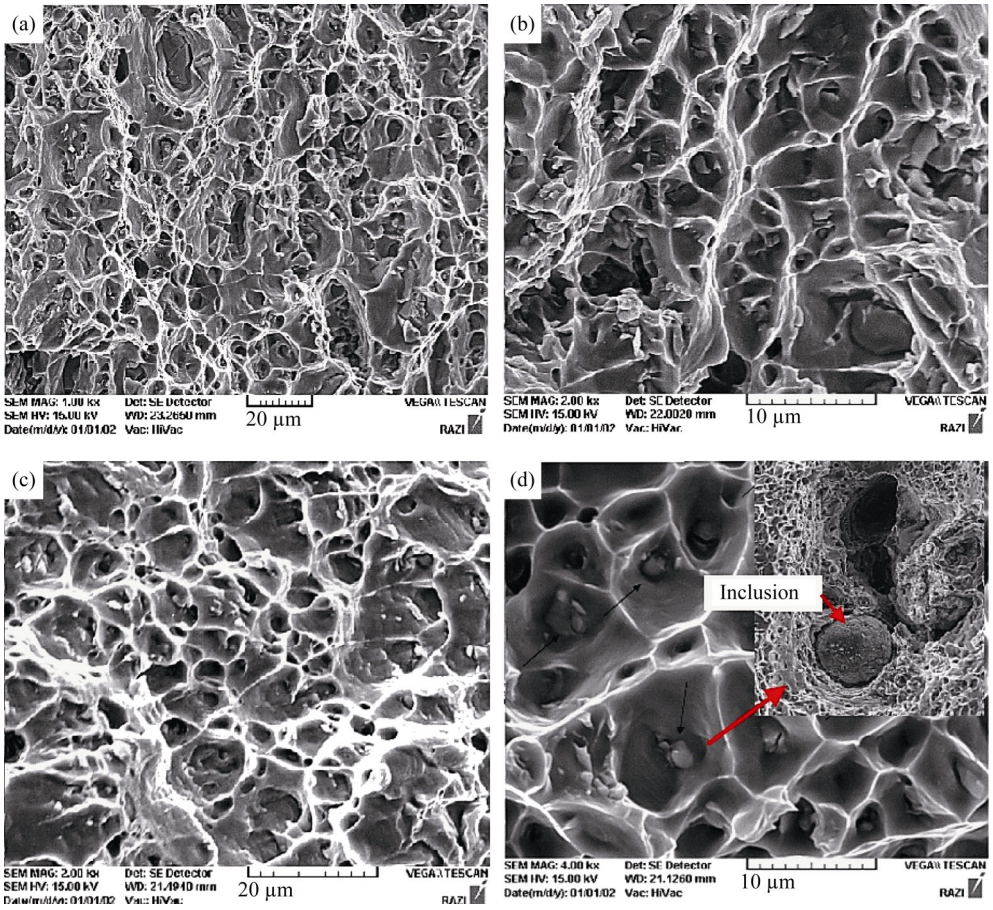

Fig. 13. SEM images of fracture surfaces as a function of nitrogen and oxygen contents in Ar shielding gas: (a) Ar–0.03vol%NO; (b) Ar–0.1vol%N_2–0.1vol%O_2; (c) Ar–1vol%N_2–2vol%O_2; (d) Ar–2vol%N_2–2vol%O_2.

also shows that the fracture surface included small inclusions with increasing N_2 and O_2 content in the shielding gas.

We conducted three-point bending tests to investigate the strength of bonding of samples welded using different shielding-gas compositions. Notably, the samples were bent as far as 180°. The bent specimens are shown in Fig. 14. These test results indicate that cracks formed in all of the specimens welded with different shielding gas compositions except for Ar–0.03vol%NO and Ar–0.5vol%N_2–0.5vol%O_2. Fig. 14 shows that, among the samples, those welded using the Ar–0.03vol%NO and Ar–0.5vol%N_2–0.5vol%O_2 shielding gases were not separated when bent to 180°. This observation indicates that AA5083-H321 GMA welding is safely applicable if the N_2 and O_2 content in the shielding gas are low, although the mechanical properties are substantially and adversely affected at higher N_2 and O_2 contents in the shielding gas.

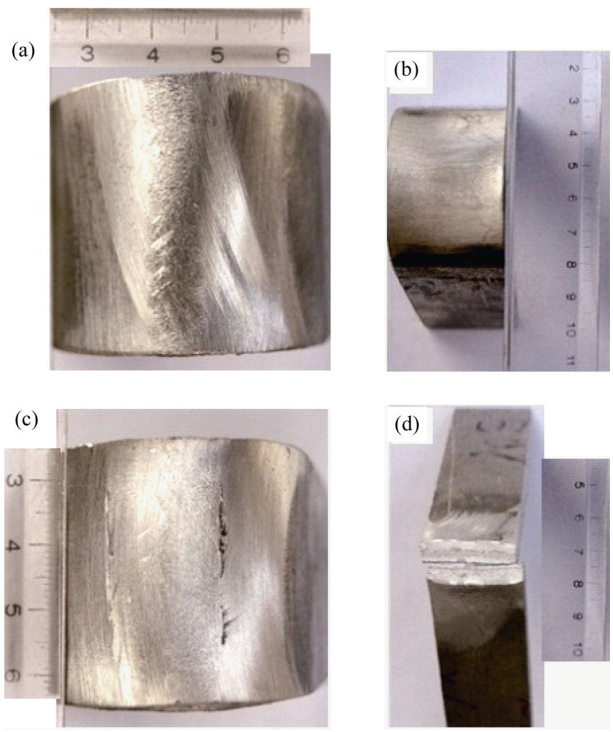

Fig. 14. Macro images of bending specimens as a function of shielding gas composition: (a) Ar–0.03vol%NO; (b) Ar–0.5vol%N_2–0.5vol%O_2; (c) Ar–1vol%N_2–1vol%O_2; (d) Ar–2vol%N_2–2vol%O_2.

4. Conclusions

DP-GMAW of 5083-H321 aluminum alloy was investigated. In this article, the influence of four different shielding gas compositions on the welding performance and properties of 5083-H321 aluminum alloy welds was studied. The results of this research led to the following conclusions:

(1) The addition of N_2, O_2, and NO to Ar shielding gas affected the solidified weld surface and the weld penetration depth. The use of Ar–0.03vol%NO as a shielding gas resulted in a clean weld bead surface.

(2) NO added to the shielding gas played a large role in inhibiting the growth of the oxide layer, resulting in a thinner oxide layer and improving the mechanical properties of the welded joints.

(3) Increasing the N_2, O_2, and NO (mixed with of Ar) contents in the weld shielding gas increased the inclusion content of the welds.

(4) The addition of N_2, O_2, and NO changed the distribution of precipitates and affected the UTS, YS (note that the tensile strength of all joints was lower than that of the base metal), and the bending test results.

References

[1] J.M. Kuk, K.C. Jang, D.G. Lee, and I.S. Kim, Effect of shielding gas composition on low temperature toughness of Al5083–O gas metal arc welds, *Sci. Technol. Weld. Joining*, 9(2004), No. 6, p. 519.

[2] I.A. Ibrahim, S.A. Mohamat, A. Amir, and A. Ghalib, The effect of gas metal arc welding (GMAW) processes on different welding parameters, *Procedia Eng.*, 41(2012), p. 1502.

[3] C.L. Mendes da Silva and A. Scotti, The influence of double pulse on porosity formation in aluminum GMAW, *J. Mater. Process. Technol.*, 171(2006), No. 3, p. 366.

[4] S. Anttila and D.A. Porter, Influence of shielding gases on grain refinement in welds of stabilized 21% Cr ferritic stainless steel, *Weld. World*, 58(2014), No. 6, p. 805.

[5] B. Mvola and P. Kah, Effects of shielding gas control: welded joint properties in GMAW process optimization, *Int. J. Adv. Manuf. Technol.*, 2016-06-01, p. 1. doi:10.1007/s00170-016-8936-2.

[6] O. Liskevych and A. Scotti, Influence of the CO_2 content on operational performance of short-circuit GMAW, *Weld. World*, 59(2015), No. 2, p. 217.

[7] H.Y. Huang, Effects of shielding gas composition and activating flux on GTAW weldments, *Mater. Des.*, 30(2009), No. 7, p. 2404.

[8] R. Prokić-Cvetković, S. Kastelec-Macura, A. Milosavljević, O. Popović, and M. Burzić, The effect of shielding gas composition on the toughness and crack growth parameters of AlMg4, 5Mn weld metals, *J. Min. Metall. B*, 46(2010), p. 193.

[9] Z. Boukha, J.M. Sánchez-Amaya, L. González-Rovira, E.D. Rio, G. Blanco, and J. Botana, Influence of CO_2–Ar mixtures as shielding gas on laser welding of Al–Mg alloys, *Metall. Mater. Trans. A*, 44(2013), No. 13, p. 5711.

[10] B. Arivazhagan, S. Sundaresan, and M. Kamaraj, A study on influence of shielding gas composition on toughness of flux-cored arc weld of modified 9Cr–1Mo (P91) steel, *J. Mater. Process. Technol.*, 209(2009), No. 12-13, p. 5245.

[11] A.B. Murphy, M. Tanaka, S. Tashiro, T. Sato, and J.J. Lowke, A computational investigation of the effectiveness of different shielding gas mixtures for arc welding, *J. Phys. D*, 42(2009), No. 11, art. No. 115205.

[12] J.M.G. de Salazar, A. Soria, and M.I. Barrena, The effect of N_2 addition upon the MIG welding process of duplex steels, *J. Mater. Sci.*, 42(2007), No. 13, p. 4892.

[13] A. Durgutlu, Experimental investigation of the effect of hydrogen in argon as a shielding gas on TIG welding of austenitic stainless steel, *Mater. Des.*, 25(2004), No. 1, p. 19.

[14] D.D. Nage, V.S. Raja, and R. Raman, Effect of nitrogen addition on the microstructure and mechanical behavior of 317L and 904L austenitic stainless steel welds, *J. Mater. Sci.*, 41(2006), No. 7, p. 2097.